JOURNAL OF COMPUTATIONAL PHYSICS **136,** 298–307 (1997)
ARTICLE NO. CP975732

SPH and Riemann Solvers

J. J. Monaghan

Department of Mathematics, Monash University, Clayton, Victoria 3168, Australia

Received May 3, 1996; revised April 21, 1997

Smooth particle hydrodynamics (SPH) is usually based on equations derived from the momentum and thermal energy equations of fluid dynamics. Artificial viscosity is added to these equations to handle shocks. In this paper we show how the equations may be formulated using the specific energy equation instead of the thermal energy equation. The resulting equations are very similar to the equations constructed for Riemann solutions of compressible gas dynamics. In particular the artificial viscosity is analogous to terms constructed from signal velocities and jumps in variables across characteristics. When applied to shock tubes, blast waves, wall shocks, and the Roberts and Sjögreen problems the new equations give very good results. They also provide the basis for the generalization of SPH to relativistic flows. © 1997 Academic Press

1. INTRODUCTION

Riemann-based solutions of the equations of compressible gas dynamics have achieved spectacular successes. The most recent example is the simulation of ultra relativistic flow using an Eulerian formulation [6, 5].

The disadvantage of Riemann-based solutions is that the Riemann problem must be solved anew when the equation of state is changed and, in physically complicated problems, this is a substantial undertaking. No Riemann solutions have yet been obtained for the important class of problems where chemical reactions occur and more than one phase exists. Even for the simple case of an isentropic two-dimensional Riemann problem, where four constant states meet at a common corner there are 16 different possible configurations (77 if the discontinuities are across two nonparallel lines), and some of these are unstable [15]. Fortunately the higher dimensional ideal gas Riemann problem can be approximated accurately by a succession of one-dimensional problems (see, for example [6]) although it is not clear what the situation is for other fluids and other configurations. A further consideration is that some Riemann methods do not handle flows where large regions of low density are suddenly created, as in the Sjögreen test [3], and they produce significant errors when a shock moves slowly through the finite difference mesh [1, 13]. Other defects of Riemann methods are discussed by Quirk [14] 1994.

Particle methods such as SPH (for a review see [8]) have advantages for many complex problems but they do not achieve the accuracy of Riemann-based methods for most ideal gas problems. However, because SPH is Galilean invariant the solution of the Roberts problem presents no difficulties, and the Sjögreen test is also handled without difficulty provided the summation form of the density is used. It would clearly be desirable to improve the ability of SPH to simulate other ideal gas problems without compromising its flexibility and this is the aim of the present paper. We focus on the dissipative terms in the SPH equations and relate them to those appearing in Riemann formulations. While the correspondence is not exact we are led to consider dissipative terms which are similar to those already used in SPH calculations and to work with the specific energy equation rather than the thermal energy equation. The resulting SPH equations give good results for a variety of gas dynamic problems and their extension to special relativistic gas dynamic also gives very good results [10].

2. THE SPH EQUATIONS

The SPH equations describe the motion of interplating points which can be thought of as particles. Each particle carries a mass m, a velocity $\mathbf{v}$, and other properties, depending on the problem.

The momentum equation for particle a is

$$\frac{d\mathbf{v}_a}{dt} = -\sum_b m_b \left(\frac{P_a}{\rho_a^2} + \frac{P_b}{\rho_b^2} + \Pi_{ab} \right) \nabla_a W_{ab}, \qquad (2.1)$$

where the summation is over all particles other than particle a (although in practice only near neighbours contribute), P is the pressure, and ρ is the density. Π_{ab} produces a shear and bulk viscosity, W_{ab} is the interpolating kernel, and ∇_a denotes the gradient of the kernel taken with respect to the coordinates of particle a. The kernel is a function of $|\mathbf{r}_a - \mathbf{r}_b|$, so that its gradient can be written

$$\nabla_a W_{ab} = \mathbf{r}_{ab} F_{ab}, \qquad (2.2)$$

where F_{ab} is a scalar function which is symmetric in a and b, and $\mathbf{r}_{ab}$ denotes $(\mathbf{r}_a - \mathbf{r}_b)$ (this notation for vectors is

0021-9991/97 $25.00

used throughout this paper). The forces between particles are therefore along the line of centres and both linear and angular momentum are conserved.

The usual form of Π_{ab} is given by the rule:

If $\mathbf{v}_{ab} \cdot \mathbf{r}_{ab} < 0$ then

$$\Pi_{ab} = -\alpha \frac{h \mathbf{v}_{ab} \cdot \mathbf{r}_{ab}}{\bar{\rho}_{ab} |\mathbf{r}_{ab}|^2} \left(\bar{c}_{ab} - 2 \frac{h \mathbf{v}_{ab} \cdot \mathbf{r}_{ab}}{|\mathbf{r}_{ab}|^2} \right), \tag{2.3}$$

else

$$\Pi_{ab} = 0,$$

where c is the speed of sound, $\bar{c}_{ab} = \frac{1}{2}(c_a + c_b)$, $\bar{\rho}_{ab} = \frac{1}{2}(\rho_a + \rho_b)$, and $\alpha \sim 1.0$ is a parameter. A parameter β that normally appears in (2.3) has been given the value 2α which numerical experiments on a wide range of fluids show is a good choice and a cutoff parameter η^2, which is usually added to $|r_{ab}|^2$ to prevent singularities [11, 8], has been removed because it is unnecessary. The parameter h determines the resolution [8] and when each particle has its own h (determined by the local density) the h used in (2.3) is $0.5(h_a + h_b)$.

This viscosity term was constructed in the following way: The term involving the speed of sound was based on the viscosity of an ideal gas. The term involving $(\mathbf{v}_{ab} \cdot \mathbf{r}_{ab})^2$ was constructed to prevent penetration in high Mach number collisions by producing an artificial pressure roughly proportional to ρv^2. The viscosity is Galilean invariant, it vanishes for rigid rotation, and it guarantees that the entropy change due to the dissipation is positive definite.

To complete the dynamics the thermal energy equation, the continuity equation, and the equation of state must be specified. One SPH form of the thermal energy equation is

$$\frac{du_a}{dt} = \frac{P_a}{\rho_a^2} \sum_b m_b \mathbf{v}_{ab} \cdot \nabla_a W_{ab} + \frac{1}{2} \sum_b m_b \Pi_{ab} \mathbf{v}_{ab} \cdot \nabla_a W_{ab}, \tag{2.4}$$

where u is the thermal energy per unit mass, and the first term comes from the compression or expansion of the gas. It is easy to show from (2.1) and (2.4) that the total energy

$$E = \sum_a m_a \left(\frac{1}{2} \mathbf{v}_a \cdot \mathbf{v}_a + u_a \right) \tag{2.5}$$

is conserved.

In an SPH calculation the density can be found by a sum over particles, but in this paper (with the exception of the Sjögreen test) we solve the continuity equation

$$\frac{d\rho}{dt} = -\nabla \cdot (\rho \mathbf{v}) + \mathbf{v} \cdot \nabla \rho, \tag{2.6}$$

which can be approximated by

$$\frac{d\rho_a}{dt} = \sum_b m_b (\mathbf{v}_a - \mathbf{v}_b) \cdot \nabla_a W_{ab}. \tag{2.7}$$

For the Sjögreen test we also calculate ρ_a from

$$\rho_a = \sum_b m_b W_{ab}. \tag{2.8}$$

Particles are moved according to

$$\frac{d\mathbf{r}_a}{dt} = \mathbf{v}_a.$$

In order to make our equations look more like those used for Riemann problems we replace the thermal energy equation by an equation for the energy $\hat{e}$ per unit mass where

$$\hat{e} = \tfrac{1}{2} v^2 + u \tag{2.9}$$

and then, in the absence of dissipation,

$$\frac{d\hat{e}}{dt} = -\frac{1}{\rho} \nabla \cdot (P \mathbf{v}). \tag{2.10}$$

One SPH form of (2.10) which includes the effect of dissipation is

$$\frac{d\hat{e}_a}{dt} = -\sum_b m_b \left(\frac{P_a \mathbf{v}_b}{\rho_a^2} + \frac{P_b \mathbf{v}_a}{\rho_b^2} + \Omega_{ab} \right) \cdot \nabla_a W_{ab}, \tag{2.11}$$

where the dissipation term Ω_{ab}, which we will discuss below, is symmetric in the properties of a and b. The total energy,

$$E = \sum_a m_a \hat{e}_a, \tag{2.12}$$

is then conserved since $\nabla_a W_{ab}$ is antisymmetric in a and b.

We do not add any terms to the continuity equation because SPH, unlike the Eulerian Riemann solvers, does not need such terms. As a result contact discontinuities are preserved very well by SPH.

3. RELATION TO RIEMANN SOLUTIONS

In order to determine the form of Π_{ab} and Ω_{ab} we consider the numerical method of Martí *et al.* [5]. Starting with the equations written in conservation form,

$$\frac{\partial \mathbf{s}}{\partial t} + \frac{\partial \mathbf{f}}{\partial x} = 0, \tag{3.1}$$

a simple Euler scheme for their numerical solution is

$$\mathbf{s}_j^{n+1} = \mathbf{s}_j^n - \frac{\Delta t}{\Delta x}\left(\tilde{\mathbf{f}}(\mathbf{s}_j, \mathbf{s}_{j-1}) - \tilde{\mathbf{f}}(\mathbf{s}_{j-1}, \mathbf{s}_j)\right); \tag{3.2}$$

Martí *et al.* [5] define numerical fluxes by

$$\tilde{\mathbf{f}}(\mathbf{s}_L, \mathbf{s}_R) = \frac{1}{2}\left(\mathbf{f}_L + \mathbf{f}_R - \sum_{i=1}^{3} |\tilde{\lambda}_i|\, \Delta\tilde{\omega}\mathbf{e}_i\right), \tag{3.3}$$

where L and R stand for the left and right states of a given interface. The λ_i are the eigenvalues (with dimensions of velocity), $\mathbf{e}_i$ are the eigenvectors of the Jacobian matrix,

$$\mathbf{A} = \frac{\partial \mathbf{f}(\mathbf{s})}{\partial \mathbf{s}}, \tag{3.4}$$

and $\tilde{\lambda}_i$ denotes an average of λ for the left and right states. The quantities $\Delta\omega$ are the jumps of the independent variables across the characteristics and they are given by

$$\mathbf{s}_R - \mathbf{s}_L = \sum_{i=1}^{3} \Delta\tilde{\omega}_i \tilde{\mathbf{e}}_i. \tag{3.5}$$

For ideal gases the eigenvalues for one-dimensional problems are v, $v + c$, and $v - c$, the last two being the signal speeds for sound propagation as seen in the frame where the fluid velocity is v.

To construct an appropriate form of Π_{ab} and Ω_{ab} for the particles a and b we treat the particles as the equivalent of left and right states and we focus on changes along the direction joining the particles. With (3.2) and (3.3) in mind we need the equivalent of the eigenvalues, that is, a signal velocity $v_{\mathrm{sig}}(a, b)$ and a jump in the relevant physical variable to correspond to the jump across characteristics. For Π_{ab} we assume the jump in the velocity across characteristics can be replaced by the velocity difference between the two particles taken along the line joining them. This is $\mathbf{v}_{ab}\cdot\mathbf{j}$, where

$$\mathbf{j} = \frac{\mathbf{r}_{ab}}{|\mathbf{r}_{ab}|}. \tag{3.6}$$

The form of the term corresponding to those involving $|\tilde{\lambda}_i|\,\Delta\tilde{\omega}_i$ in (3.3) is then

$$v_{\mathrm{sig}}(a, b)\mathbf{v}_{ab}\cdot\mathbf{j}.$$

However, because the pressure terms in the summation of (2.1) have an extra density in the denominator arising from the SPH interpolation, the expression for Π_{ab} we are led to is

$$\Pi_{ab} = -\frac{K v_{\mathrm{sig}}(a, b)\mathbf{v}_{ab}\cdot\mathbf{j}}{\bar{\rho}_{ab}}, \tag{3.7}$$

where K is an arbitrary constant which we expect to be ~ 1 and the sign of the expression for Π_{ab} is determined by the fact that when particles are approaching we want Π_{ab} to be positive and therefore equivalent to an increase in effective pressure. When $\mathbf{v}_{ab}\cdot\mathbf{r}_{ab} > 0$ we set Π_{ab} to zero. The form of $v_{\mathrm{sig}}(a, b)$ will be discussed later, but we note for the present that if we were to choose

$$v_{\mathrm{sig}}(a, b) = c_a + c_b - 2\mathbf{v}_{ab}\cdot\mathbf{j}$$

and $K = 0.5\alpha$ the viscosity term would be identical to (2.3), except that $\mathbf{j}$ in (3.7) replaces $h\mathbf{r}_{ab}/|\mathbf{r}_{ab}|^2$ in (2.3).

In the case of the energy equation we need the jump in energy so we assume Ω has the form

$$\Omega_{ab} = -\frac{K v_{\mathrm{sig}}(a, b)(\hat{e}_a - \hat{e}_b)\mathbf{j}}{\bar{\rho}_{ab}}, \tag{3.8}$$

but in turns out that, to ensure positive definite viscous dissipation, we should replace $\hat{e}$ by e^*, where

$$e_a^* = \tfrac{1}{2}(\mathbf{v}_a\cdot\mathbf{j})^2 + u_a. \tag{3.9}$$

This is also consistent with our picture of properties taken with respect to the line joining the two particles. Ω_{ab} is set to zero for separating particles.

The momentum and energy equation then take the form

$$\frac{d\mathbf{v}_a}{dt} = -\sum_b m_b\left(\frac{P_a}{\rho_a^2} + \frac{P_b}{\rho_b^2} - \frac{K v_{\mathrm{sig}}(a, b)}{\bar{\rho}_{ab}}\mathbf{v}_{ab}\cdot\mathbf{j}\right)\nabla_a W_{ab} \tag{3.10}$$

and

$$\frac{d\hat{e}_a}{dt} = -\sum_b m_b\left(\frac{P_a\mathbf{v}_b}{\rho_a^2} + \frac{P_b\mathbf{v}_a}{\rho_b^2} - \frac{K v_{\mathrm{sig}}(a, b)}{\bar{\rho}_{ab}}(e_a^* - e_b^*)\mathbf{j}\right)\cdot\nabla_a W_{ab}. \tag{3.11}$$

If desired, the thermal energy equation for particle a can then be constructed by first differentiating (2.9) which gives

$$\frac{du_a}{dt} = \frac{d\hat{e}_a}{dt} - \mathbf{v}_a \cdot \frac{d\mathbf{v}_a}{dt}. \tag{3.12}$$

Then, using (3.10) and (3.11), we find

$$\frac{du_a}{dt} = \frac{P_a}{\rho_a^2} \sum_b m_b \mathbf{v}_{ab} \cdot \nabla_a W_{ab} + \sum_b m_b \frac{K v_{\mathrm{sig}}(a,b)}{\bar{\rho}_{ab}} (\mathbf{j}(e_a^* - e_b^*) - \mathbf{v}_a(\mathbf{v}_{ab} \cdot \mathbf{j})) \cdot \nabla W_{ab}. \tag{3.13}$$

Replacing $\nabla_a W_{ab}$ using (2.2) and substituting for e^* in the second summation in (3.13), we find

$$\frac{du_a}{dt} = \frac{P_a}{\rho_a^2} \sum_b m_b \mathbf{v}_{ab} \cdot \mathbf{r}_{ab} F_{ab} + \sum_b m_b \frac{K v_{\mathrm{sig}}(a,b)}{\bar{\rho}_{ab}} \left(u_a - u_b - \frac{1}{2} (\mathbf{v}_{ab} \cdot \mathbf{j})^2 \right) |\mathbf{r}_{ab}| \mathbf{F}_{ab}. \tag{3.14}$$

The contribution to the change in the thermal energy of particle a from velocity terms (this is the viscosity contribution) is, therefore,

$$-\frac{1}{2} \sum_b m_b \frac{K v_{\mathrm{sig}}(a,b)(\mathbf{v}_{ab} \cdot \mathbf{j})^2}{\bar{\rho}_{ab} |\mathbf{r}_{ab}|} F_{ab}, \tag{3.15}$$

which is positive definite since $F_{ab} \leq 0$. If we had used the true specific energy rather than e^* we could not have guaranteed that the viscous contribution to the thermal energy would be positive definite. The remaining contribution to the change of thermal energy of particle a is

$$\sum_b m_b \frac{|\mathbf{r}_{ab}| K v_{\mathrm{sig}}(a,b)}{\bar{\rho}_{ab}} (u_a - u_b) F_{ab}, \tag{3.16}$$

which is similar to a standard SPH form of the thermal conduction equation [8, 9]. Note that if u_a in (3.9) is replaced by $f u_a$, where f is a parameter, the thermal conductivity is multiplied by f.

4. THE SIGNAL SPEED

The signal velocities for the Lagrangian form of the one-dimensional equations of ideal gas dynamics are given by Whitehurst [18] using Toro's results (based on Godunov's second method [4]). There are two signal velocities and they depend on the solutions of an intermediate state. Toro [16] writes the Riemann solution in terms of left and right uniform states. The motion of the fluid creates an intermediate state with pressure p^*. We define $H_L = p_L/p^*$. The signal velocity for the left state is then given by the following rule (obtained from the Hugoniot relations), where the velocity is positive if from the left to the right state: if $H_L \leq 1$ then

$$\lambda_L = v_L + c_L; \tag{4.1}$$

else

$$\lambda_L = v_L + c_L \left(1 + \frac{(\gamma - 1)(H_L - 1)}{2\gamma} \right)^{1/2}, \tag{4.2}$$

with a similar rule for λ_R the signal speed at the right state. In the Riemann solvers H_L is found from the equations of gas dynamics.

The quantity we have called $v_{\mathrm{sig}}(a, b)$ is an effective signal velocity. It is the speed of approach of two signals, one from a towards b and one from b towards a. This is the natural speed for the sharing of physical quantities such as velocity and energy.

For convenience think of a as the left state and b as the right state along a line joining the two particles. The velocity of a signal from a to b is then λ_a which we write in the form

$$c_a + \mathbf{v}_a \cdot (-\mathbf{j}), \tag{4.3}$$

and the velocity of a signal sent from b to a is λ_b and, taking account of the directions, this can be written

$$-c_b + \mathbf{v}_b \cdot (-\mathbf{j}). \tag{4.4}$$

When both H_a and H_b are ≤ 1, $v_{\mathrm{sig}}(a, b)$ is the difference of these two signal velocities and this is

$$v_{\mathrm{sig}}(a,b) = c_a + c_b - \mathbf{v}_{ab} \cdot \mathbf{j}. \tag{4.5}$$

Note that if the two particles are approaching $\mathbf{v}_{ab} \cdot \mathbf{j} < 0$ so that $v_{\mathrm{sig}}(a, b) \geq 0$, when it is used.

In the general case the intermediate Riemann state must be computed [16, 4]. Our intention here, however, is not to solve the Riemann problem but merely to use it as a guide to improve SPH. The equation that Toro uses for the intermediate state shows that this state depends on the relative velocities along the line of sight. In the case of strong shocks we find that the term involving H_L in (4.2) is proportional to $(v_L - v_R)^2/c_L^2$. We therefore guess that, in place of (4.1) and (4.2), it would be reasonable to estimate λ_L by the single approximate formula

$$\lambda_L = v_L + (c_L^2 + \beta(v_L - v_R)^2)^{1/2}, \tag{4.6}$$

where β is a parameter that could be determined by numerical experiments. With this approximation, following the argument that led to (4.5), we get

$$v_{\rm sig}(a,b) = (c_a^2 + \beta(\mathbf{v}_{ab}\cdot\mathbf{j})^2)^{1/2} + (c_b^2 + \beta(\mathbf{v}_{ab}\cdot\mathbf{j})^2)^{1/2} - \mathbf{v}_{ab}\cdot\mathbf{j}. \tag{4.7}$$

The signal velocity (4.7) is similar to the signal velocity which produces the standard SPH dissipative terms (described after (3.7)). Furthermore, when inserted in the acceleration equation, it produces an artificial pressure which is similar to that discussed by Dukowicz [2] who also noted the relation between artificial viscosities and solutions of the Riemann problem. In a related discussion Wilkins [17] used the solution for strong and weak shocks to estimate the parameters for artificial viscosities. In our numerical experiments we used both (4.7) and, following Dukowicz [2], the approximation

$$v_{\rm sig} = c_a + c_b - 3\mathbf{v}_{ab}\cdot\mathbf{j} \tag{4.8}$$

which does not require square roots. However, in our experiments we only use the signal velocity terms for approaching particles and the extra time involved in using (4.7) is negligible.

The Courant condition must depend on $v_{\rm sig}(a,b)$ because this is the speed at which information between the states is sent and it is time to construct a new state when the signal from a to b meets the signal from b to a. We therefore assume the local time step is given by

$$\delta t = \frac{\sigma h}{v_{\rm sig}(a,b)}, \tag{4.9}$$

where $\sigma \sim 1$ is a constant determined by numerical experiment but it is applicable to a wide range of gases, solids, and liquids. This time-step rule is almost identical to the condition used by Whitehurst [18] for his free lagrange method, except he replaces h by the distance between cell faces. In the calculations described later the minimum of the local time steps is used as actual time step.

The time-step condition (4.9) is similar to that already used in previous SPH calculations where the time step was constructed by combining a time step based on the speed of sound and one based on the viscosity. This meant that, instead of (47), the previous SPH calculations used a close approximation to

$$v_{\rm sig}(a,b) = c_a + c_b - \mathbf{v}_{ab}\cdot\mathbf{j}, \tag{4.10}$$

and $\sigma \sim 0.3$.

The arguments presented in this and the previous section are no more than heuristic. It is difficult to present an analytical argument directly relating the properties of the Riemann solution to those of the SPH equations because of the differences between finite difference methods and particle methods. As remarked earlier, the usual line of argument for the SPH viscosity is to use the known viscosity of a gas and other physical and computational considerations, such as designing the quadratic viscosity to prevent penetration of particle streams [7] while knowing that it also has the property of giving constant thickness shocks for gas dynamics. However, in the case of relativistic flow, it is not clear what is the appropriate form of the dissipation and the heuristic arguments of the present paper prove invaluable in designing the viscosity.

As a consequence of these considerations we take the point of view that the validity of our heuristic arguments can be determined by applying the equations to a wide variety of numerical experiments. Applications of the present ideas to ultra relativistic flow are given elsewhere [10].

5. NUMERICAL TESTS

In the following numerical experiments, which involve variants of shock tubes, we integrate the acceleration, energy and the continuity equations using a second-order predictor–corrector method and the time step (4.9) with $\sigma = 1$. The numerical integration conserves total energy and momentum to within the roundoff error.

In these tests we use the spline based kernel with continuous second derivatives [8]. In all cases the resolution length h for the kernels was allowed to vary with density according to the rule $h \propto 1/\rho$. When calculating the kernels and their derivatives we use the average $h = 0.5(h_a + h_b)$. The initial value of h_a was 1.5 the initial particle spacing at the position of particle a.

When an initial physical quantity A is discontinuous it was smoothed according to the rule

$$A = \frac{A_L + A_R e^{x/d}}{1 + e^{x/d}}, \tag{5.1}$$

where A_L denotes the uniform state to the left of the origin, A_R is the uniform state to the right of the origin, and d is taken as half the largest initial particle separation at the interface.

Since we use equal mass particles higher densities are associated with closer particle spacing and, when the density is smoothed, it means the spacing and, therefore, the initial h must be smoothed. In the case of the shock tube the spacing changes by a factor of 8 across the initial interface and if this is not smoothed the evolution is very badly corrupted. This might be expected since SPH is based on smoothing of the equations of motion.

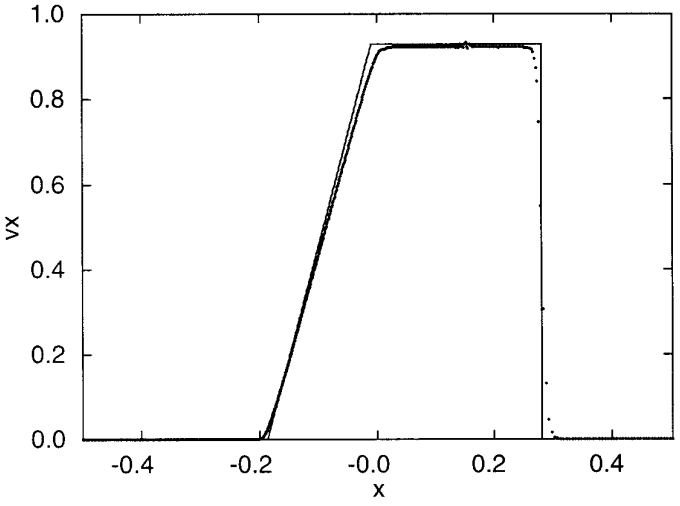

FIG. 1. Velocity against distance for the shock tube. The particle spacing to the right of the initial interface is 0.005.

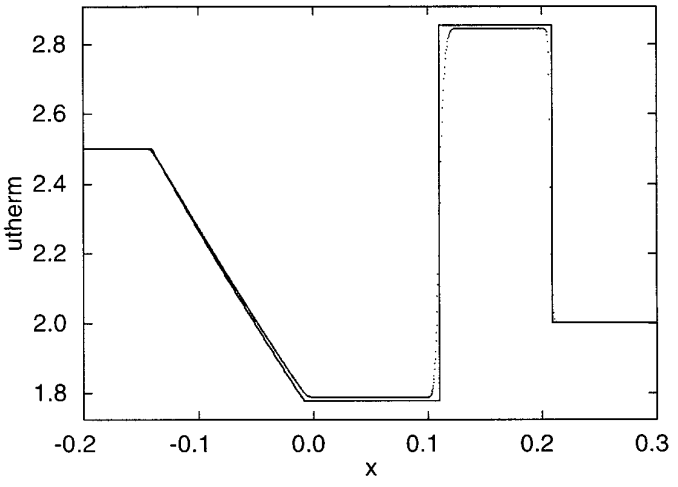

FIG. 3. Thermal energy against distance for the shock tube with particle spacing 0.005.

When the initial density is smoothed the particles were spaced according to the rule

$$\rho_a(x_{a+1} - x_{a-1}) = 2\rho_R \Delta_R, \tag{5.2}$$

where ρ_R is the density of the fluid to the far right of the origin where the particle spacing is Δ_R.

Shock Tube

Figures 1 to 3 show results for the standard Sod shock tube test calculated using the signal velocity (4.7) (with $\beta = 1$). To reduce the thermal diffusion we take $f = 0.50$ (see the remarks after (3.16)). The initial state consists of static gas with $\gamma = 1.4$, and $u = 2.5$ and $\rho = 1$ for $x < 0$, and $u = 2.0$ and $\rho = 0.125$ for $x > 0$. The initial particle spacing is 0.005 for particles with $x > 0$. The particle spacing elsewhere is determined according to (5.2).

The velocity distance graph shows that there are negligible oscillations behind the shock and a good rarefaction wave. The shock front is several particles wide but because the spacing varies by a factor 2 the shock width is three initial particle spacings.

The SPH velocity behind the shock is 0.922, compared with the exact value of 0.926. There is a small variation of the velocity for those particles which were close to the initial discontinuity in density and pressure. The density distance graph shows nearly identical resolution of the shock and contact discontinuity. The density behind the shock is 0.265 (exact value 0.265) and behind the contact discontinuity it is 0.432 (exact value 0.425). The thermal energy reaches a peak value of 2.84 (exact value 2.85) and a minimum value 1.788 (exact value 1.781). Similar results were obtained for values of β in the range $1 < \beta < 4$.

In Figs. 4, 5, and 6 we show the results for the same parameters except the particle spacing for $x > 0$ is 0.001. The difference between the computed and exact results is negligible.

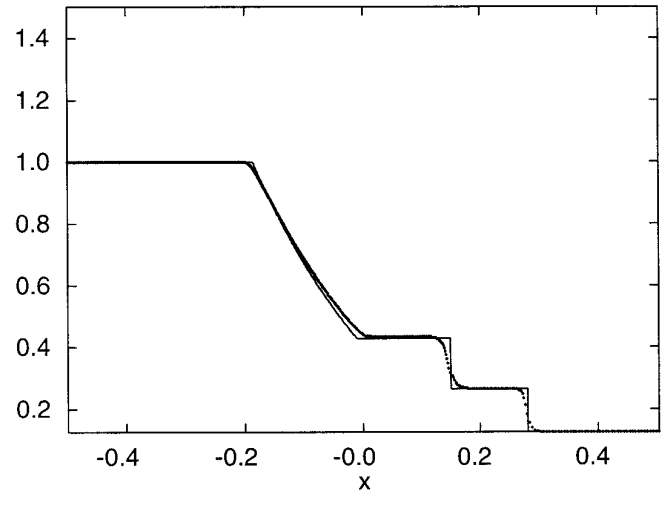

FIG. 2. Density gradient distance for the shock tube with particle spacing 0.005.

Blast Wave

In Figs. 7 and 8 we show the density and velocity for one section of the blast wave considered by Woodward and Colella [19]. This is a diffcult test because the velocity of the contact discontinuity is close to the shock velocity producing a sharp spike in the density behind the shock.

The initial state is an ideal gas at rest with $\rho = 1$, $\gamma = 1.4$, and $P = 1000$ for $x < 0$ and $\rho = 1$ and $P = 0.01$ for $x > 0$. We smooth the initial thermal energy to give a

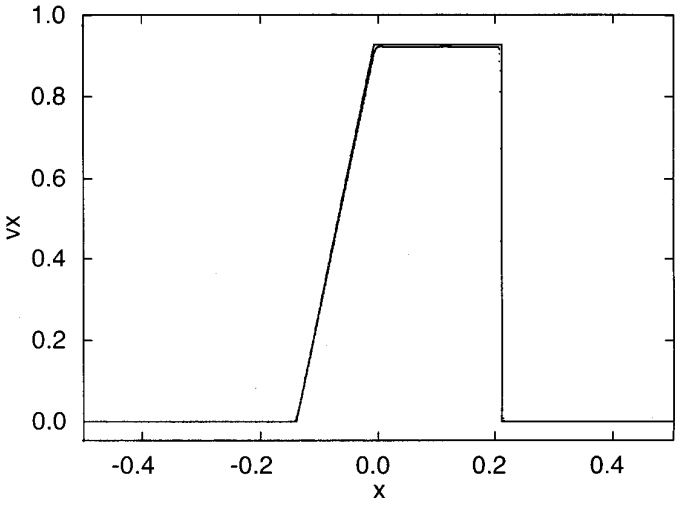

FIG. 4. Velocity against distance for the shock tube with particle spacing to the right of the initial interface 0.001.

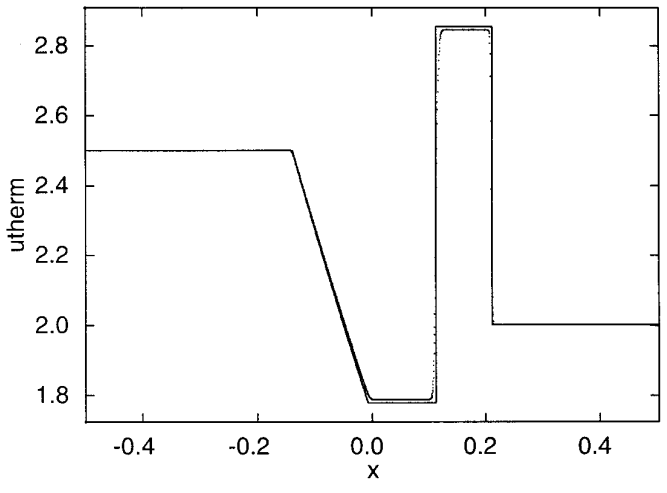

FIG. 6. Thermal energy against distance for the shock tube with particle spacing 0.001.

smooth $\hat{e}$. For the results shown here the initial particle spacing was 0.001, $K = 0.5$, $f = 0.5$, and for the calculation of v_{sig} we took $\beta = 1$. The velocity graph shows a disturbance at the contact discontinuity but is otherwise very close to the theoretical values. The density graph shows that the spike is overestimated by about 10%, but the remainder of the density is reproduced very well.

The rule used for a symmetric h is $0.5(h_a + h_b)$. Alternative rules for producing a symmetric h for the interaction between pairs of particles produced very similar results for the velocity and thermal energy but the density spike had a different value. For example, if h for particles a and b is chosen by the rule $2h_a h_b/(h_a + h_b)$ then the spike is underestimated by 10%. If, on the other hand, when h_a is decreasing, it is not allowed to decrease by more than 10% in a step, then the error in the spike is less than 2%. The velocity and thermal energy then have errors slightly larger (2%) than for the original rule for h.

Wall Shock

In Figs. 9, 10, and 11 we show the velocity, density, and thermal energy for a configuration consisting of two cold streams with oppositely directed velocities. This problem is the equivalent of one stream of gas striking a wall. The Riemann-based solutions have an advantage for this problem because they produce the correct initial state. The SPH calculation proceeds by converting the kinetic energy at the interface between the two streams into thermal en-

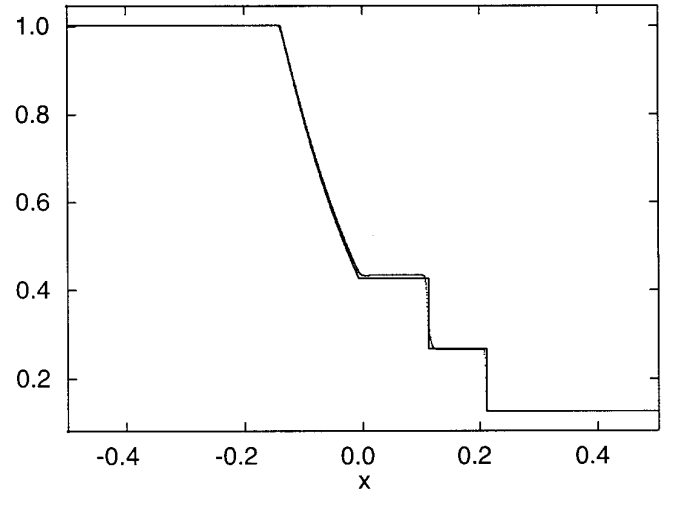

FIG. 5. Density against distance for the shocktube with particle spacing 0.001.

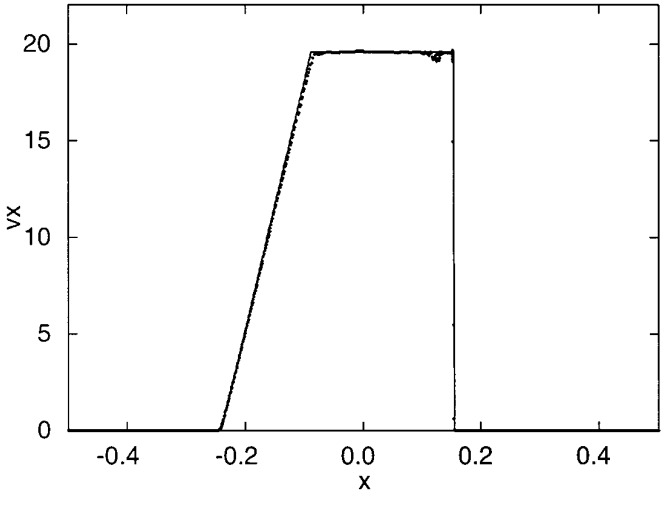

FIG. 7. Velocity against distance for the blast wave with initial particle spacing 0.001.

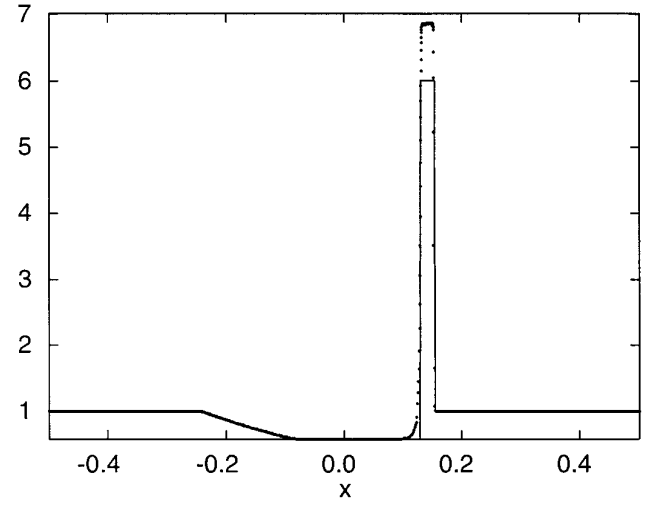

FIG. 8. Density against distance for the blast wave with initial spacing 0.001. Notice that the density jump at the shock is in error by 10%. The error can be reduced to 2% by limiting the change of h.

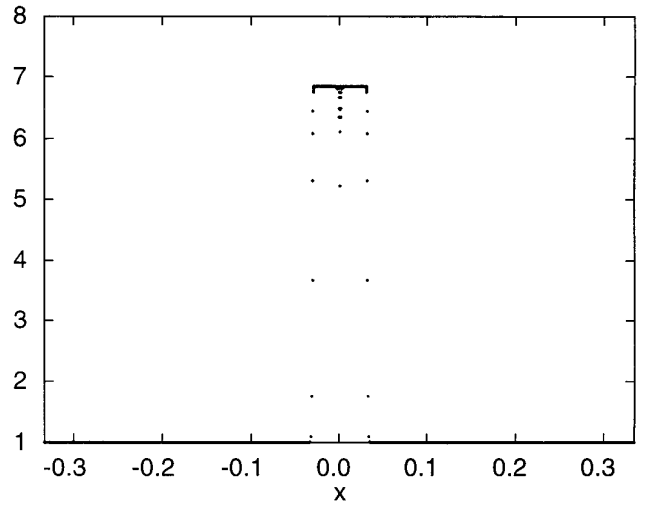

FIG. 10. Density against distance for the wall shock. Note the presence of the inverse spike at the position of the initial interface and the flatness of the postshock region elsewhere. The density jump is in error by 10%. The error is reduced to 2% when the change of h is limited.

ergy and the simulation shows a thermal spike. In the calculations shown here we have smoothed the initial discontinuous velocity field but the spike is still significant. The calculations use the same values of K, β, γ, and f as before with initial particle spacing 0.001, $\rho = 1$, $|v| = 1$, and $u = 10^{-6}$.

Figure 9 shows that the velocity is obtained accurately with a sharp shock and negligible ripples. Figure 10 shows that the density variation which, apart from the downward spike at the interface, has a post shock value which is too large by 10%. As with the blast wave this error is virtually eliminated if h is not allowed to decrease by more than 10% in a step. The thermal energy shown in Fig. 11 also has a spike at the interface but it is much smaller relative to the postshock value than the density spike. Apart from the spike the postshock thermal energy is within 1% of the exact value.

Roberts Problem

As remarked earlier the Roberts problem [12] exposes a weakness of some linear Riemann solvers when solving problems where a shock moves through the mesh very slowly (see the discussion by Colella and Woodward [1]). The Riemann solvers produce long wavelength noise downstream which degrades the solution. Because SPH is

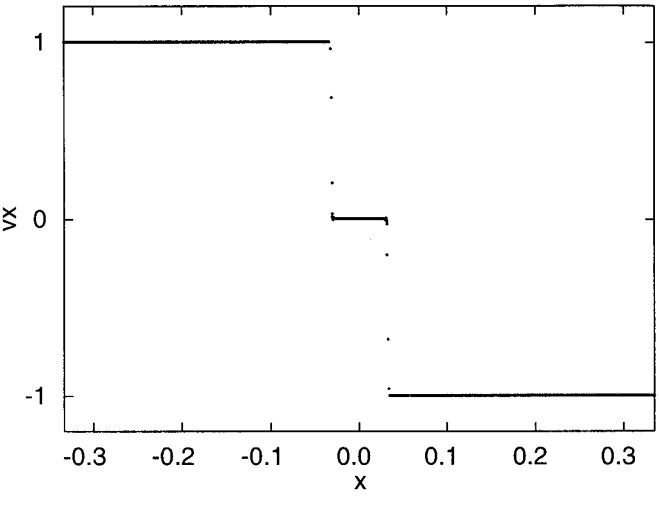

FIG. 9. Velocity against distance for the wall shock with initial particle spacing 0.001.

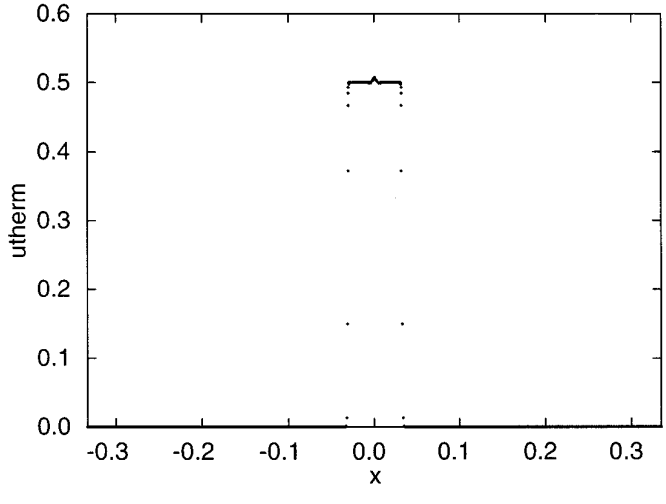

FIG. 11. Thermal energy against distance for the wall shock. Note the small spike at the interface. The exact post shock value is 0.5.

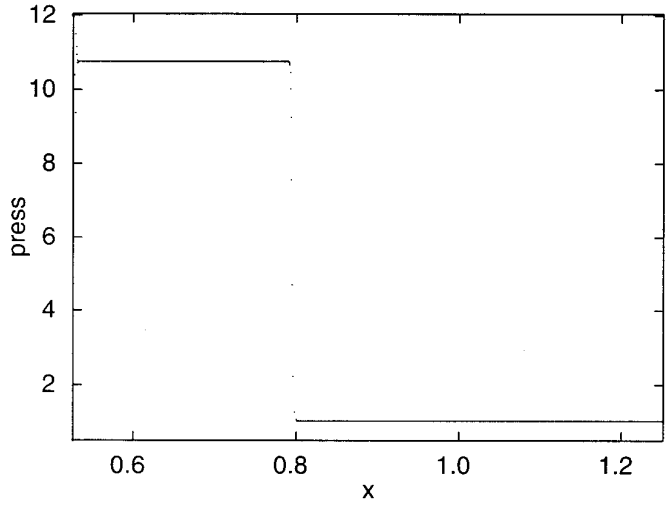

FIG. 12. The pressure–distance relation for the Roberts problem. Note the absence of long wave length noise in front of the shock.

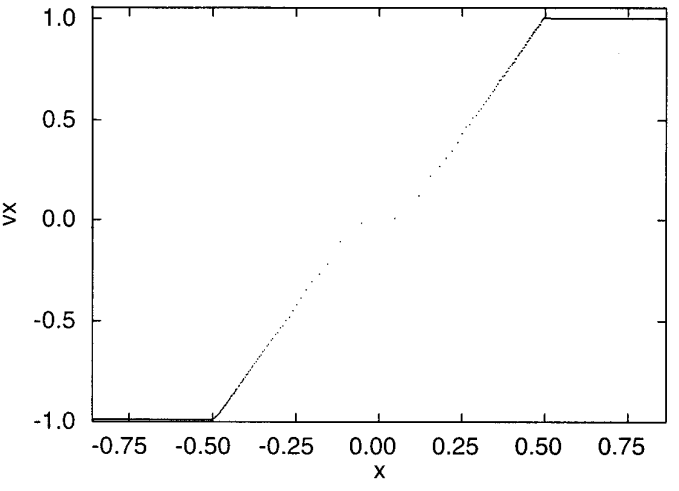

FIG. 13. The velocity–distance relation for the Sjögreen test. Note the straight lines of the velocity profiles arising from the rarefactions and the plateau where they join.

Galilean invariant and has no mesh, there is no difficulty with this problem. Nevertheless to show the quality of the results with the present algorithm we show the pressure-distance graph in Fig. 12. The initial configuration is the same as that used by Xu *et al.* [20] that is (preshock velocity, density, and pressure of $(-3.44, 1.0, 1.0)$ and postshock $(-0.81, 3.86, 10.33)$ with $\gamma = 1.4$. This produces a Mach 3 shock which, for a Courant number of 1.0, takes 50 steps to move through a cell of a finite difference mesh. With our code we can, if desired, add a constant velocity to the original state without changing the results. The results as indicated by Fig. 12 are comparable to those found by Xu *et al.* [20].

Sjögreen Test

The Sjögreen test was discussed by Einfeldt *et al.* [3]. They showed that no linearized Riemann solution can be positively conservative. We choose the same initial state as that considered by Xu *et al.* [20]. To the left (velocity, density, and pressure) are $(-2, 1, 0.4)$ and on the right $(2, 1, 0.4)$. The velocity was not smoothed at the interface.

When this simulation was first run the results were very bad. This was traced to the continuity equation. When (2.7) was replaced by (2.8) the problem disappeared. If the summation is used for every time step the calculation takes about 30% longer than if the continuity equation is integrated, because it requires an extra pass over the cells to provide the pressure and density required for the force calculation. To reduce the cpu time experiments were performed with the calculation of the density via the continuity equation, alternating with that calculated by the summation. The resulting velocity profile is shown in Fig. 13. The exact solution consists of the classical rarefaction straight lines joining a plateau. The SPH results are excellent. In Fig. 14 we show the density and this is in good agreement with the results of Xu *et al.* [20] although the minimum density is always limited by the contribution of an SPH particle's mass to its own density. The thermal energy profile is very good, except in the central region where it is larger than the exact values which are close to zero.

If the summation is used every step the results are slightly better.

6. DISCUSSION AND CONCLUSIONS

The results of these calculations show that working with the momentum and energy equation, and basing the dissi-

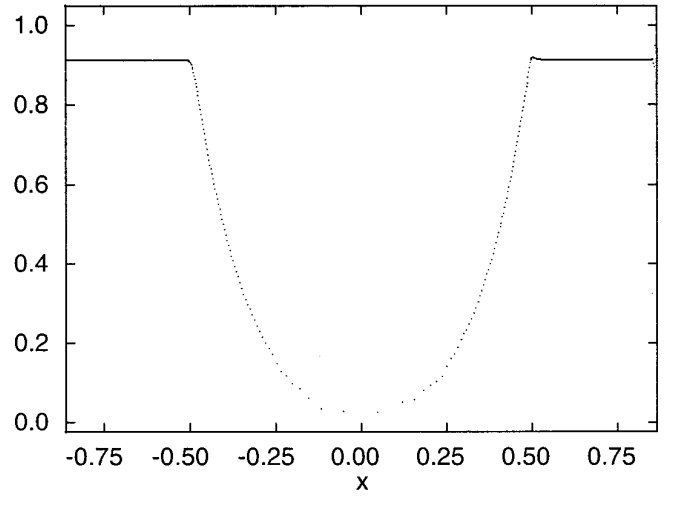

FIG. 14. The density–distance relation for the Sjögreen test. Note the characteristic U shape of the density profiles arising from the rarefactions and the fact that the central density remains positive.

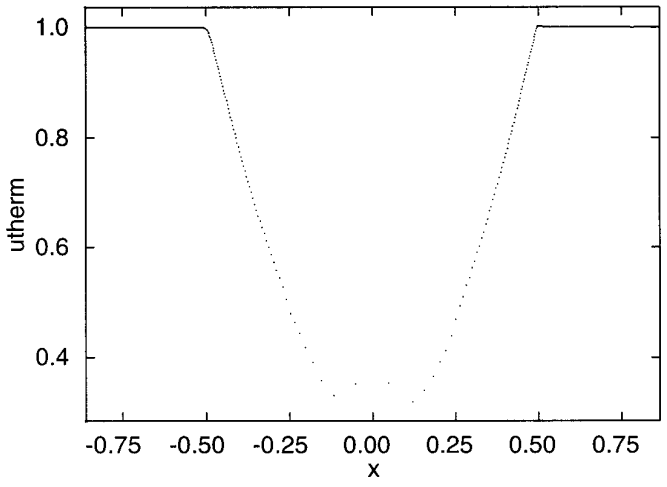

FIG. 15. The thermal energy-distance relation for the Sjögreen test. Note the slight jump in the thermal energy in the central region.

pative terms on those used in Riemann solvers, gives good results for a wide variety of gas dynamic problems. The results for the shock tube, blast wave, and wall shocks are, in general, not as good as those obtained using the exact, or well approximated, Riemann solutions but this is to be expected because those solutions compute the exact jumps across characteristics. As a result the SPH shock fronts are broader than those for Riemann based solutions. Nevertheless the results are comparable to those of Dukowicz [2], giving better rarefractions but poorer shocks, and similar to Whitehurst's second-order method. The most significant errors occur in infinite strength shocks where the calculated density jump is too high.

Because of its Galilean invariance the SPH solution of the Roberts problem presents no difficulties and the results are as good as the gas-kinetic finite volume methods of Xu *et al.* [20]. Problems involving large regions with low densities, as in the Sjögreen test, where two sections of the fluid move apart, present significant difficulties for Riemann methods but our SPH algorithm can handle them easily, provided the summation form of the density equation is used.

Whitehurst notes differences between SPH and his Lagrangian Flame method. Some of these differences are essential and some are not essential. For example, in a count of the arbitrary constants in the SPH dissipation terms he includes the cutoff parameter η which is unnecessary (see the remark after (2.3)). Whitehurst also criticises the two artificial viscosity terms used in SPH but the present calculations show that they occur quite naturally and consistently from the signal velocity. Furthermore, the parameters used are those that are to be expected from the signal velocity and, when a parameter such as β in (4.4) cannot be estimated accurately without solving the Riemann problem, it turns out to have very little effect on the calculations. As with Whitehurst's method the time step follows immediately from the signal velocity and is in close agreement with the time step rules already used. The main advantage of SPH over Flame is that SPH is much simpler to program, has much less storage, and can be used for complex problems where the Riemann solution is not known.

The method described here has been extended to ultra relativistic fluid dynamics [10] with good results. We can also expect that it will provide a good basis for dissipative terms in MHD problems. Finally we note that because all the equations in this paper are in vector form they can be applied immediately to multidimensional problems.

REFERENCES

1. P. Colella and P. Woodward, *J. Comput. Phys.* **54** (1984), 174.
2. J. K. Dukowicz, *J. Comput. Phys.* **61** (1985), 119.
3. B. Einfeld, C. D. Munz, P. L. Roe, and B. J. Sjögreen, *J. Comput. Phys.* **92** (1991), 273.
4. J. J. Gottlieb and C. P. T. Groth, *Comput. Phys.* **78** (1988), 437.
5. J. *Mª* Martí, J. M. Ibáñez, and J. A. Miralles, *Phys. Rev. D* **43** (1991), 3794.
6. J. *Mª* Martí and E. Müller, *Comput. Phys.* **123** (1996), 1.
7. J. J. Monaghan and R. A. Gingold, *J. Comput. Phys.* **52** (1983), 374.
8. J. J. Monaghan, *Ann. Rev. Astron. Astrophys.* **30** (1992), 543.
9. J. J. Monaghan, *Heat conduction with discontinuous thermal conductivity,* Mathematics Dept., Monash University, App. Math. 1995/18.
10. J. J. Monaghan and E. Chow, Ultra Relativistic SPH, *J. Comput. Phys.,* in press.
11. J. J. Monaghan and R. A. Gingold, *J. Comput. Phys.* **52** (1983), 374.
12. J. P. Morris and J. J. Monaghan, *A Shock Switch for SPH,* Mathematics Dept., Monash University, 1996.
13. T. W. Roberts, *J. Comput. Phys.* **90** (1990), 141.
14. J. J. Quirk, *Int. J. Num. Methods in Fluids* **18** (1994), 141.
15. C. W. Schultz-Rinne, J. P. Collins, and H. M. Glaz, *SIAM J. Sci. Statist. Comput.* **14** (1993), 1394.
16. E. G. Toro, *Phil. Trans. A. Roy. Soc.* **341** (1992), 499.
17. M. L. Wilkins, *J. Comput. Phys.* **36** (1980), 281.
18. Whitehurst, *Mon. Not. R. Astron. Soc.* **277** (1995), 655.
19. P. Woodward and P. Collela, *J. Comput. Phys.* **54** (1984), 115.
20. K. Xu, L. Martinelli, and A. Jameson, *J. Comput. Phys.* **120** (1995), 48.